Michigan State University

National Superconducting Cyclotron Laboratory

PROJECTILE-LIKE FRAGMENT MOMENTUM DISTRIBUTIONS FROM ^{86}Kr + Al AT 70 MeV/NUCLEON

R. PFAFF, D.J. MORRISSEY, M. FAUERBACH, M. HELLSTRÖM, J.H. KELLEY, R.A. KRYGER, B.M. SHERRILL, M. STEINER, J.S. WINFIELD, J.A. WINGER, S.J. YENNELLO, and B.M. YOUNG

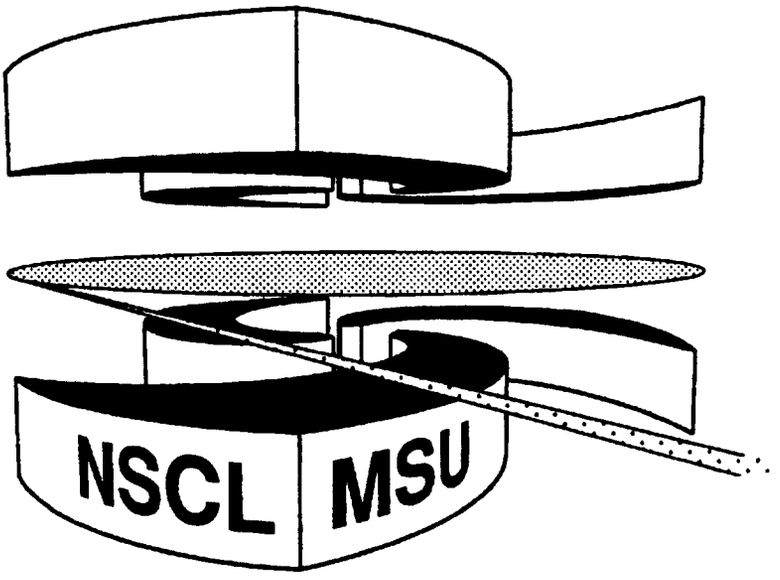

MSUCL-957 NOVEMBER 1994

Projectile-like fragment momentum distributions from ^{86}Kr + Al at 70 MeV/nucleon

R. Pfaff[1,2], D.J. Morrissey[2,3], M. Fauerbach[1,2], M. Hellström[2], J.H. Kelley[1,2], R.A. Kryger[2], B.M. Sherrill[1,2], M. Steiner[1,2], J.S. Winfield[2,*], J.A. Winger[2,†], S. J. Yennello[2,‡], and B.M. Young[1,2,§]

[1] *Department of Physics and Astronomy, Michigan State University, East Lansing, MI 48824*

[2] *National Superconducting Cyclotron Laboratory, Michigan State University, East Lansing, MI 48824*

[3] *Department of Chemistry, Michigan State University, East Lansing, MI 48824*

Abstract

Projectile-like residue yields and momentum distributions from the reaction of 70 MeV/nucleon ^{86}Kr with ^{27}Al at 0° were studied. The data is compared with a model developed originally for higher energies (> 200 MeV/nucleon), data from prior experiments performed at both higher and lower bombarding energies, and a semi-empirical parameterization derived from high energy systematics.

25.70.Mn, 27.30.+t

I. INTRODUCTION

Projectile fragmentation has proven to be an effective method to produce a broad range of exotic nuclei. The production of near-beam velocity projectile-like fragments (PLF's) is relatively well understood in both the high energy (E > 200 MeV/nucleon) and low energy (E < 20 MeV/nucleon) domains. At relativistic energies 'pure' projectile fragmentation occurs and is generally considered to proceed via a two-step process [1]. In the first stage a highly excited prefragment is formed as independent nucleons are removed from the projectile during a rapid interaction with the target. A slow deexcitation step follows and involves particle evaporation to produce the final observed projectile residue. The excitation energy distribution of the prefragments is an important parameter in several different models that predict the outcome of the fragmentation process. Often the excitation energy is adjusted to fit the experimental data. The microscopic intranuclear cascade model (INC) [2] typically predicts larger excitation energies than does the macroscopic abrasion-ablation model [3], where often the excitation energies of the prefragments are more than doubled to reproduce the experimental yields. A more recent statistical abrasion model [4] combines both the microscopic and macroscopic viewpoints, treating the overlap region of the nuclear interaction on a purely statistical basis.

Reactions in the low energy domain include many competing processes such as transfer reactions, direct breakup, and pickup reactions. Inelastic processes occur which can lead to highly excited prefragments. Many experiments have been performed to map out the low energy reaction processes [5,6]. However, the situation in the transitional intermediate energy domain (20 MeV/nucleon < E < 200 MeV/nucleon) is not well understood, primarily due to the limited availability of experimental data, particularly for reactions involving medium-mass and heavy-mass nuclei. The present experiment was performed in the intermediate energy region with a relatively heavy projectile in an effort to study the transition between the low and high energy phenomena and to clarify which processes contribute to the total reaction yields in this region. Results of the present work are compared with both

the INC-based ISApace model [7] and the semi-empirical EPAX parameterization [8] based on data from many high energy experiments. From a practical standpoint, it is crucial for the planning of future experiments with secondary beams that the production yields of the most exotic nuclei produced in intermediate energy reactions be accurately predicted. Both the ISApace model and EPAX parameterization are routinely used to describe various properties of experimental data involving PLF production. The gradual transition from the deep inelastic processes of the low-energy regime to the 'pure' fragmentation at relativistic energies must be systematically mapped out to gain a better understanding of the interplay between the competing reaction mechanisms present in the intermediate energy region.

II. EXPERIMENTAL PROCEDURE

The measurements were performed at the National Superconducting Cyclotron Laboratory using a $\sim$ 0.1 pnA ^{86}Kr beam at 70 MeV/nucleon delivered by the K1200 cyclotron. The beam was incident on a 4 mg/cm^2 ^{27}Al target placed at the medium acceptance target position of the A1200 mass separator [9] (see figure 2 in Ref. [9]). The angular acceptance for fragments was $\Delta\theta$ = 34 mrad and $\Delta\phi$ = 30 mrad centered around 0°, and the momentum acceptance was Δp/p = $\pm$ 1.5 %. The thickness of the target was chosen to limit the broadening of the fragment momentum distributions induced by energy and angular straggling in the target, rather than to optimize the production rate of specific fragments. The magnetic rigidity of the separator was varied in overlapping steps of 2% covering a range from $B\rho$ = 2.40 to 2.85 Tm, corresponding to projectile residue mass-to-charge ratios A/Q = 1.96 to 2.33. Four beam monitor detectors mounted around the target position in a cloverleaf pattern enabled normalization of the beam current for data taken at different rigidity settings.

The velocity of each particle was determined from the time-of-flight (TOF) measured between two 8 mg/cm^2 plastic scintillators separated by a 14 m flight path. The timing scintillators were located at the first dispersive image and the focal plane of the A1200.

The position and angle of reaction products were measured at both the second dispersive image and at the focal plane with two pairs of X-Y position sensitive parallel plate avalanche counters (PPAC's) [10] separated by approximately 40 cm. For each particle, the position information at the second dispersive image PPAC was used together with NMR measurements of the A1200 dipole fields to determine its magnetic rigidity $B\rho$, which is linearly related to the particle momentum. Reaction products reaching the focal plane were implanted into a four-element silicon detector telescope, consisting of two 300 μm ΔE detectors followed by two 1000 μm thick E detectors. All four detectors had an active area of 300 mm^2. The two energy-loss measurements provided redundant proton number (Z) determinations. By transporting charge states of the primary beam through the A1200 at different rigidity settings the relationship between the magnetic rigidity and the horizontal position at the second dispersive image was calibrated. Using the values of ΔE, total kinetic energy, TOF, and magnetic rigidity it is possible to unambiguously determine the mass (A), proton number (Z), and charge state (Q) of individual isotopes using the following relationships:

$$Z = a + b \cdot \sqrt{\Delta E \cdot (\gamma - 1)} \tag{1}$$

$$Q = \frac{3.1077}{931.5} \cdot \frac{E_{kin} \cdot \beta\gamma}{B\rho \cdot (\gamma - 1)} \tag{2}$$

$$A = \frac{Q \cdot B\rho}{3.1077 \cdot \beta\gamma} \tag{3}$$

where a and b are constants dependent on the gain of the individual ΔE detectors, E_{kin} is the total kinetic energy of the particle (in MeV), γ and β are the usual relativistic parameters, and $B\rho$ is the measured magnetic rigidity (in Tm). The measurements had resolutions (FWHM) of $\Delta A/A \sim 0.3$, $\Delta Z/Z \sim 0.4$, and $\Delta Q/Q \sim 0.3$, which allowed clear separation of all the fragments. The good charge resolution allowed an integer value of Q to be used to calculate the fragment mass. Momentum distributions were obtained for sixty-three individual projectile-like fragments of elements ranging from arsenic (Z=33) to yttrium (Z=39).

III. RESULTS AND DISCUSSION

The parallel momentum distribution of each isotope was fitted with a Gaussian function from which the parallel momentum width and the mean momentum transfer were obtained. The isotopic yield was extracted by integrating the Gaussian fit over momentum space. The projectile-like fragment momentum distributions at this energy are generally asymmetric, with a tail on the low-momentum side of the momentum distribution. The Gaussian functions were fitted to the data with a least-squares technique from $\sim 50\%$ of the peak height on the low momentum side to the end of the high momentum side of the distribution. The effect of changing the cut-off percentage on the low momentum side was explored. A typical momentum distribution is shown in Fig. 1 along with Gaussian fits done with varying cut-off percentages on the low momentum side of the distribution. The figure indicates that the width of the distribution becomes narrower as the cut-off increases toward the top of the peak. We have selected the 50% cut as the best representation of the data for subsequent discussion. The parameters that describe the data are summarized in the next sections.

A. Momentum widths

In the Goldhaber model [11], the removal of independent nucleons from the projectile results in a Gaussian momentum distribution. The width of this distribution is given by the expression

$$\sigma_{\parallel} = \sigma_o \cdot \sqrt{\frac{A_F(A_P - A_F)}{A_P - 1}} \tag{4}$$

where A_F is the fragment mass, A_P is the projectile mass, and σ_o is a reduced width related to the Fermi momenta of the individual nucleons ($\sigma_0{}^2 = p_{Fermi}^2/5$). This model reproduces the parallel momentum distribution widths of the PLF's relatively well for high energy fragmentation, and for light ion fragmentation at intermediate energies. However, the experimental value of σ_0 is typically found to be smaller than the values predicted using known Fermi momenta. Several arguments have been presented to explain the observed narrowing of the

width. One possibility is that Pauli exclusion effects could lead to a decreased width [12], while another argument [13] points out the fact that the width predicted by the Goldhaber model is relevant to the prefragments - not the final observed fragments. The prefragments will undergo a particle evaporation step leading to mass loss but little increase in momentum width (given isotropic evaporation), thereby yielding momentum widths smaller than expected. Our measured values of the parallel momentum widths in the projectile rest frame are shown in Fig. 2. The best fit to our data using the Goldhaber model, corresponding to σ_0 = 124 MeV/c, is indicated by the solid line. By interpolating results obtained in a quasi-elastic electron scattering measurement [14], we obtain a value of p_{Fermi} = 260 MeV/c for ^{86}Kr which translates into a $\sigma_0 \sim$ 116 MeV/c. Also shown in Fig. 2 are the results from calculations with the ISApace code [7] fit with the Goldhaber model (dotted line). This approach yields a reduced width of $\sigma_0 \sim$ 100 MeV/c which is also smaller than the value obtained with our data. The dot-dash line in Fig. 2 shows a calculation based on the systematics of Morrissey [15] that were obtained from parameterization of high energy fragmentation data. The parallel momentum width in this parameterization is given by

$$\sigma_{||} = constant \cdot \sqrt{\Delta A} \tag{5}$$

where $\Delta A = A_P - A_F$ and the constant is generally between 85 - 100 MeV/c. The best fit to our data requires a constant of 120 MeV/c, which is again larger than the typical value determined from high energy fragmentation. Values of the reduced width obtained from other experiments involving krypton fragmentation at various energies [13,16,17] are summarized in Fig. 3. The values of the reduced width for both the 200 MeV/nucleon and 500 MeV/nucleon data were obtained by applying a best fit with the Goldhaber model while limiting the fit to the fragment range covered in the present work. The experiments performed at higher energies (^{84}Kr at 200 MeV/A [16] and ^{86}Kr at 500 MeV/A [13]) have best fit values of $\sigma_0 \sim$ 100 MeV/c and $\sigma_0 \sim$ 90 MeV/c, respectively. After applying a 50% cut to the $^{72}Ge^{31+}$ momentum distribution shown in Fig. 4 by Bazin *et al.* [17] we estimate that $\sigma_0 \sim$ 130 MeV/c for the 44 MeV/nucleon ^{86}Kr + ^{27}Al data. Applying an 80% cut to

the low energy side of the momentum distribution yields a value of $\sigma_0 \sim 105$ MeV/c. Fig. 3 shows that the reduced width observed during heavy-ion fragmentation exhibits a definite broadening as the projectile energy is lowered into the intermediate energy regime. This is in contrast to fragmentation involving light and intermediate mass projectiles (A$\leq$40) where the general trend shows a relatively constant reduced width until the intermediate energy range is reached, where the reduced width begins to decrease smoothly [18].

The large parallel momentum distribution widths observed in the present data are probably due to the coexistence of competing reaction mechanisms in the intermediate energy regime. Apart from the 'pure' fragmentation component (that completely dominates at higher energies), both the low-energy tail typical of more dissipative processes [19] and the broadening associated with nucleon pick-up reactions during the formation of the prefragment [20] will increase the distribution width. The value of $\sigma_0 \sim 124$ MeV/c was obtained with a cut-off at 50% of the peak height on the low momentum side of the momentum distribution. It should be noted that as the momentum distributions begin showing tails on the low momentum side for experiments performed in the intermediate and low energy regimes, various assumptions have to be made about the effect of the low energy tail. Qualitative decisions have been made on how much of the tail to include and this, of course, can lead to different interpretations of data. In the present data, Gaussian fits including the entire tail yield a value of $\sigma_o \sim 130$ MeV/c while placing the cut-off at 80% of the peak height yields a value of $\sigma_o \sim 115$ MeV/c. Performing a fit exclusively with the high energy side of the momentum distribution (i.e. a 100% cut-off) yields a value of $\sigma_0 \sim 105$ MeV/c, although the fit is rather qualitative (see Fig. 1).

B. Momentum transfer

Morrissey [15] has defined average parallel momentum transfer $< P'_{||} >$ as the product of the projectile mass, the average measured velocity of the fragment $< \beta_{||} >$, and a kinematic factor of $\beta\gamma/(\gamma + 1)$, and has shown that a linear relationship exists between $< P'_{||} >$ and

the product of the total number of nucleons removed from the projectile ΔA, with a slope parameter of 8 MeV/c. This dependence was derived from high energy fragmentation data. The average parallel momentum transfer $< P'_{||} >$ for the present data is presented in Fig. 4. Changing the Gaussian fit cut-off percentage on the momentum tail has a relatively small effect on the determination of the parallel momentum transfer, introducing an uncertainty of $\sim$ 2% (the shift of the Gaussian centroid can be seen in Fig. 1) which was added in quadrature to the statistical uncertainty. The solid line in Fig. 4 is the result of a linear fit to all the fragment data with Z $\leq$ 36. The resulting slope parameter of 8.8 MeV/c is in good agreement with the overall trend of the fragmentation products (Z $\leq$ 36), while the pick-up products (solid symbols in Fig. 4) differ significantly from this trend. Recent measurements [16] at E=200 MeV/nucleon have a similar slope for the overall fit to the fragmentation products while the slopes of the individual elements exhibit deviations from this trend.

The momentum transfer for the individual elements is shown in Fig. 5 together with the results of a calculation using the ISApace code [7] (denoted by asterisks) which shows good agreement with the present data. The solid lines represent the average fitted slope parameter of 8.8 MeV/c. As is evident from Fig. 5, the slopes of the individual fragmentation elements (Z $\leq$ 36) are slightly steeper than the 8.8 MeV/c average slope, with linear best-fit slope parameters for the individual elements change monotonically as shown in Fig. 6. This effect indicates that a larger excitation energy is required to produce the proton-rich isotopes causing a greater downshift in momentum relative to the neutron-rich isotopes. Recent data from krypton fragmentation at 500 MeV/nucleon [13] showed a very similar effect, with the slope parameters of the PLF's being larger than 8.8 MeV/c. However, the slope parameters of Ref. [13] increase strongly as the proton number decreased from Z = 36 (14 MeV/c) to Z = 30 (58 MeV/c). An increased slope parameter for individual elements was also observed in xenon fragmentation at 790 MeV/nucleon [21] where the data yielded a slope of $\sim$ 16 MeV/c for the near-projectile elements.

More interesting are the parallel momentum transfers of the charge pick-up products which deviate significantly from those of the fragmentation products. The formation of the

pick-up products (in this case with Z > 36) is assumed to take place during the initial prefragment formation when individual protons are acquired from the target nucleus. The final observed fragment is then formed through neutron evaporation. Another possible production mechanism is the excitation of a Δ-resonance that can change the isospin of a projectile nucleon. However, our ISApace calculations indicate that for ^{86}Kr fragmentation at 70 MeV/nucleon this effect can account for no more than 0.5% of the total charge pick-up products. Using momentum conservation arguments similar to those used by Souliotis *et al.* [20], we can determine the momentum shift arising purely from picking up protons. Initially the projectile has a momentum p_P with a mass A_P and the proton in the target has a momentum of p_t. After the collision the prefragment has a momentum of p_{PF} and a mass of $A_p + \Delta A_t$ where ΔA_t is the number of nucleons removed from the target. Assuming the evaporation is isotropic, the average final fragment velocity (v_F) will be identical to the average velocity of the prefragment and it can then be shown that the velocity shift due to picking up the target nucleons is given by

$$\Delta\beta_{||} = \frac{1}{931.5} \cdot \frac{\Delta A_t}{A_P + \Delta A_t} \cdot (p_{Fermi} - (\frac{p_P}{A_P})) \tag{6}$$

which corresponds to a shift in the parallel momentum transfer of

$$P'_{offset} = \frac{A_P}{A_P + \Delta A_t} \cdot \frac{\beta\gamma}{\gamma + 1} \cdot \Delta A_t \cdot ((\frac{p_P}{A_P}) - p_t) \tag{7}$$

where β and γ are the relativistic parameters from the initial projectile velocity. This offset is then added to the parallel momentum transfer yielding a parameterization of the form

$$- < P'_{||} >= 8.8\frac{MeV}{c} \cdot \Delta A + P'_{offset} \cdot \Delta A_t \tag{8}$$

where the best-fit slope parameter of 8.8 MeV/c (the slope of the fragmentation products) was held fixed. Fitting the present charge pick-up data to this parameterization and adjusting the momentum of the picked-up proton(s), we obtain a value of $p_t \sim 220$ MeV/c. The results are shown with dashed lines in Fig. 4. The value obtained for the proton momentum indicates that the protons acquired during the pick-up process are moving parallel to the

projectile with approximately their maximum Fermi momentum. This effect has previously been observed in reactions involving neutron pick-up [20].

C. Isotopic Cross Sections

The absolute cross sections for the Z = 33 (arsenic) through Z = 39 (yttrium) isotopes were obtained by integrating the Gaussian fits of the parallel momentum distributions over momentum space and are shown in Fig. 7. The error bars indicate the statistical uncertainty added in quadrature to the uncertainty due to altering the fitting limits on the tail of the momentum distribution. Inclusion of the momentum distribution tail increases the cross sections by $\sim$ 8%. The absolute beam current was $\sim$ 0.1 pnA with an uncertainty of a factor of two. The relative cross sections are much more precise than this. The absolute normalization uncertainty is not included in the error bars. The solid histograms represent the calculated cross sections from the ISApace model [7], which is considered to be valid between a few hundred MeV/nucleon and a few GeV/nucleon. ISApace uses the Yariv-Fraenkel ISABEL intranuclear cascade code [22] to model the prefragment formation step followed by a modified PACE evaporation code [23] to calculate the deexcitation step. The magnitudes and shapes of the predicted isotopic cross section distributions are in remarkable agreement with the experimental data for the fragmentation products ($Z \leq 36$). In contrast, the measured cross sections of the charge pick-up products are greater than predicted by ISApace, and this difference grows as the number of acquired protons increases (although the shapes of the distributions are reproduced rather well).

Figure 7 also shows cross sections predicted from the semi-empirical parameterization (EPAX) established by Sümmerer *et al.* [8] (dotted histograms). Cross sections predicted by the EPAX code are generally higher than the observed cross sections for the neutron-rich isotopes while the proton-rich isotopes are underpredicted. This indicates that the evaporative step of the whole process contributes significantly to the proton-rich side of the isotopic chains, as expected for high excitation energies in the prefragments. Both ISApace

and EPAX underpredict the cross sections of the charge pick-up products indicating that, as expected, the high-energy models are not able to reproduce the experimental data for the charge pick-up products.

The ISApace model has previously been used to predict the cross sections for 500 MeV/nucleon ^{86}Kr fragmentation as discussed in Ref. [13]. In this case, the ISApace calculation predicted the cross sections fairly well, while the EPAX calculation showed a similar underprediction for proton-rich nuclei and overprediction of the neutron-rich nuclei that is observed for the current data at 70 MeV/nucleon. It was suggested that the Gaussian shape of the charge dispersion used in the EPAX formula needs to be modified in order to reproduce the data. In Ref. [16], the ^{84}Kr fragmentation data obtained at 200 MeV/nucleon were compared to an INC model consisting of a combination of an ISABEL code followed by the evaporation code LOTO [19]. This model accurately reproduced the most probable N/Z distribution of the observed fragments. The data were also compared to a participant-spectator model [24], but in order to reproduce the N/Z distribution peak in this case, the prefragment excitation energies had to be increased by a factor of ten before implementation of the LOTO code.

IV. CONCLUSIONS

This study of the parallel momentum width, momentum transfer, and isotopic cross sections in the intermediate energy regime indicates that a significant portion of the reaction processes are consistent with high energy fragmentation. Although the parallel momentum width is larger than expected for high energy fragmentation, the dependence of the width with mass loss is fairly well reproduced by the Goldhaber model when σ_0 is taken as a free parameter. The even larger momentum widths evident in data from 44 MeV/nucleon could be attributed to a prevalent occurrence of nucleon pick-up reactions, which could also account for the increase in widths evident in the present data. The parallel momentum transfer of the fragmentation products is very well modeled with the ISApace code and follows the general

trend of the high energy systematics developed by Morrissey. The momentum transfer of the charge pick-up products can be accurately described by assuming that additional momentum loss occurs purely because the projectile acquires excess mass as it interacts with the target. The PLF cross sections are also well reproduced by the ISApace code, with the exception of the charge pick- up products. This indicates that, apart from 'pure' fragmentation, other processes contribute significantly in the formation of charge pick-up products. The EPAX parameterization underpredicts the proton-rich side of the isotopic chains while overpredicting the neutron-rich side. This effect has also been seen in the krypton fragmentation at higher energies [13,16] where the discrepancy between observed yield and predicted yields was not as significant. The agreement with the ISApace model shows that this model can be used at this intermediate energy of 70 MeV/nucleon, while it is apparent that the EPAX parameterization needs to be modified to account for recent experimental data from heavy ion fragmentation both at high and intermediate energies.

This work was supported by the National Science Foundation under Grant number PHY-92-14922.

REFERENCES

* Present Address: 43 Hinckley Road, Leicester Forest East, Leicester LE3 3GL, Great Britain

† Present Address: Dept of Physics and Astronomy, Mississippi State University, Mississippi State, MS 39762-5167

‡ Present Address: Cyclotron Institute, Texas A&M University, College Station, TX 77843- 3366

§ Present Address: A.W. Wright Nuclear Structure Laboratory, Yale University, PO Box 6666, 272 Whitney Ave, New Haven, CT 06511

[1] R. Serber, Phys. Rev. **72** 1114 (1947).

[2] K. Chen, Z. Fraenkel, G.F. Friedlander, J.R. Grover, J.M. Miller, and Y. Shimamoto, Phys. Rev. **166** 949 (1969).

[3] D. J. Morrissey, W.R. Marsh, R.J. Otto, W. Loveland, G.T. Seaborg, Phys. Rev. **C18** (1978) 1267.

[4] T. Brohm and K.-H. Schmidt, Nucl. Phys. **A569** 821 (1994).

[5] M. Lefot and C. Ngô, Ann. de Phys. **3** 5 (1978).

[6] J.R. Birkelund and J.R. Huizenga, Ann. Rev. Nucl. Part. Sci. **33** 161 (1978).

[7] M. Fauerbach, Diploma thesis, TH Darmstadt, (1992).

[8] K. Sümmerer, W. Bruchle, D.J. Morrissey, M. Schadel, B. Szweryn, and W. Yang, Phys. Rev. **C42** 2546 (1990).

[9] B.M. Sherrill, D.J. Morrissey, J.A. Nolen Jr., and J.A. Winger, Nucl. Instrum. Methods **B56** 1106 (1991).

[10] D. Swan, J. Yurkon, and D.J. Morrissey, Nucl. Instrum. Methods **A**, in press (1994).

[11] A.S. Goldhaber, Phys. Lett. **B53** 306 (1974).

[12] G. Bertsch, Phys. Rev. Lett. **46** 472 (1981).

[13] M. Weber *et al.*, GSI-94-29 Preprint, April 1994, submitted to Nucl. Phys. **A**.

[14] E.J. Moniz, I. Sick, R.R. Whitney, J.R. Ficenec, R.D. Kephart, and W.D. Trower, Phys. Rev. Lett. **26** 445 (1971).

[15] D.J. Morrissey, Phys. Rev. **C39** 460 (1989).

[16] C. Stéphan *et al.*, Phys. Lett. **B262** 6 (1991).

[17] D. Bazin, D. Guerreau, R. Anne, D. Guillemaud-Mueller, A.C. Mueller, and M.G. Saint-Laurent, Nucl. Phys. **A515** 349 (1990).

[18] M.J. Murphy and R.G. Stokstad, Phys. Rev. C28 428 (1983).

[19] L. Tassan-Got and C. Stéphan, Nucl. Phys. **A524** 121 (1991).

[20] G.A. Souliotis, D.J. Morrissey, N.A. Orr, B.M. Sherrill, and J.A. Winger, Phys. Rev. **C46** 1383 (1992).

[21] J. Friese, H.J. Körner, J. Reinhold, R. Schneider, K. Zeitelhack, H. Geissel, A. Magel, G. Münzenberg, K. Sümmerer, Proc. of the 3rd Int. Conf. on Radioactive Nuclear Beams (East Lansing, USA, May 1993), D.J. Morrissey, Ed., Edition Frontières (Gif-sur-Yvette, France, 1993)., pg. 333.

[22] Y. Yariv and Z. Fraenkel, Phys. Rev. **C20** 2227 (1979).

[23] A. Gavron, Phys. Rev. **C21** 230 (1980).

[24] J. Gosset, H.H. Gutbrot, W.G. Meyer, A.M. Poskanzer, A. Sandoval, R. Stock, and G.W. Westfall, Phys. Rev. **C16** 629 (1977).

FIGURES

FIG. 1. A typical fragment momentum distribution. In this case $^{80}Br^{35+}$ is shown with Gaussian fits using varying cuts on the low momentum side of the distribution. The statistical error bars are smaller than the symbols representing the experimental data. The momentum per nucleon of the beam is indicated by the arrow.

FIG. 2. Widths of parallel momentum distributions as a function of mass number compared to predictions using the Goldhaber model [11] (solid line) and the systematics of Morrissey [15] (dot-dash line). The solid symbols indicate charge pick-up products. The dotted line represents the overall trend of predictions using the ISApace model [7]. The error bars represent the statistical error added in quadrature with the uncertainty due to cuts on tail of the momentum distribution. See text for details.

FIG. 3. Parallel momentum widths from previous experiments involving krypton fragmentation. The diamond indicates the data 500 MeV/nucleon data described in Ref. [13] and the circle shows the data from Ref. [16]. In both cases a Gaussian fit to the full momentum distribution was used. The square represents data from Ref. [17] where a 50% cut was used on the low momentum side of the momentum distribution. The data from the present experiment is shown by the solid circle. The error bars shown on the intermediate energy data are due to altering the cut-off percentage applied to the momentum distribution.

FIG. 4. Momentum transfer vs. mass loss (A_P - A_F). The solid line indicates the linear relationship between momentum transfer and mass loss shown by Morrissey [15]. A slope parameter of 8.8 MeV/c is the best linear fit to the fragmentation products ($Z \leq 36$). The predictions for the proton pick-up products ($Z \geq 37$) are shown with dashed lines and are calculated from a momentum conservation model (discussed in text) in which protons with a momentum oriented along the direction of the projectile motion are preferentially picked-up from the target. The error bars represent the statistical uncertainty added in quadrature with the uncertainty due to cuts on the momentum distributions.

FIG. 5. Momentum transfer of the individual elements. The solid line indicates the systematics of Morrissey [15] with a slope parameter of 8.8 MeV/c. The asterisk symbols represent the values predicted by the ISApace model. The dashed lines represent the parameterization of Eq. 8. See text for details. The error bars are smaller than the symbols representing the experimental data.

FIG. 6. Slope parameters for the individual elements. The dashed line is the best fit line of the fragmentation isotopes ($Z \leq 36$) and has a value of 12.2 MeV/c which is greater than the overall trend of the data shown in Fig. 3. See text for details.

FIG. 7. The isotopic cross sections for the elements between arsenic (Z=33) and yttrium (Z=39). The solid histograms represent predictions from the intranuclear-cascade model ISApace [7], while the dotted histograms indicate predictions from the EPAX parameterization [8]. The error bars indicate the statistical uncertainty added in quadrature with the uncertainty due to cuts on the momentum distributions.

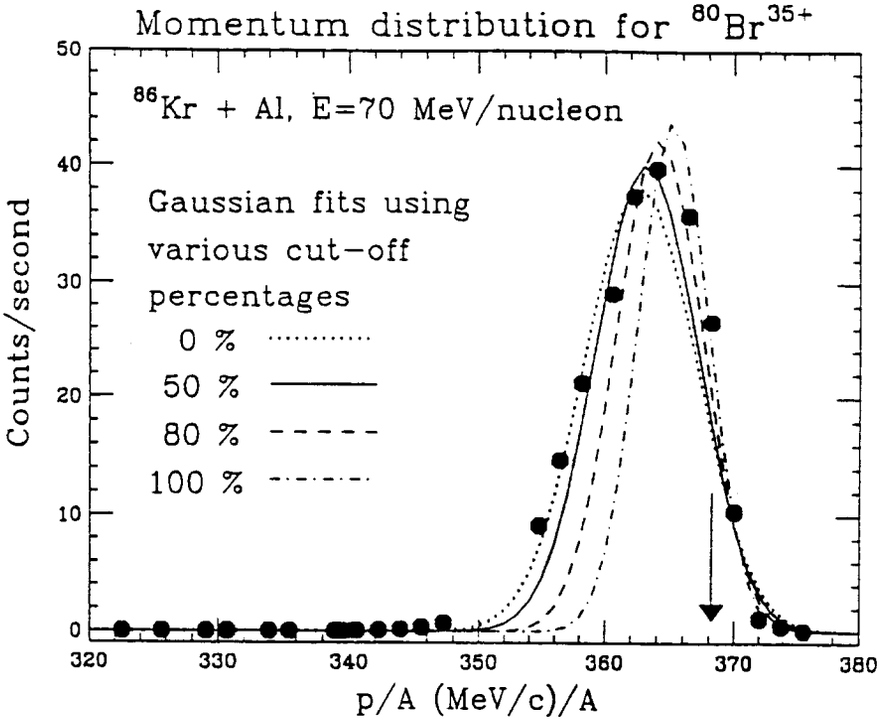
Momentum distribution for $^{80}Br^{35+}$
^{86}Kr + Al, E=70 MeV/nucleon
Gaussian fits using
various cut−off
percentages
0 %
50 %
80 %
100 %
Counts/second
p/A (MeV/c)/A

Fig. 1

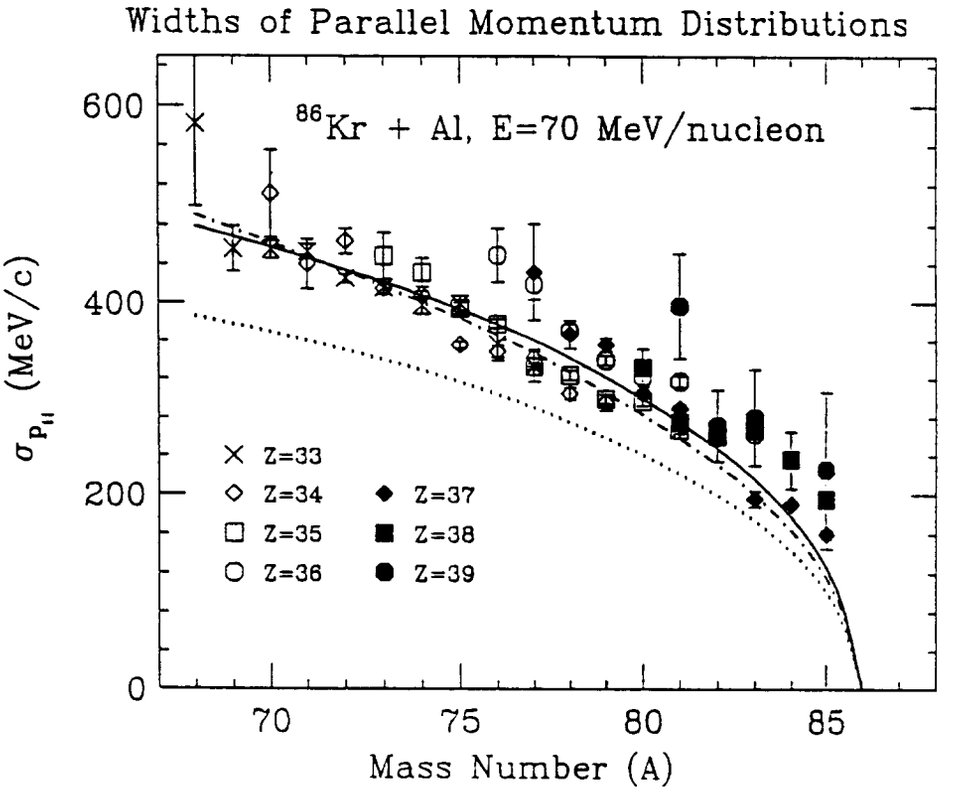
Widths of Parallel Momentum Distributions
^{86}Kr + Al, E=70 MeV/nucleon
Z=33
Z=34
Z=35
Z=36
Z=37
Z=38
Z=39
$\sigma_{P_{II}}$ (MeV/c)
Mass Number (A)

Fig. 2

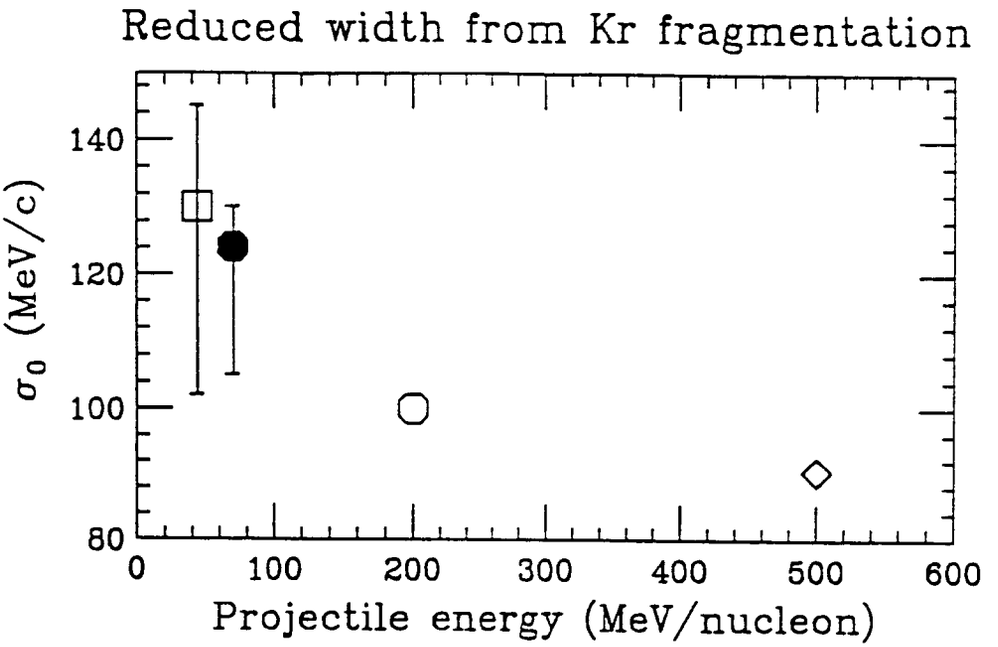
Reduced width from Kr fragmentation
σ_0 (MeV/c)
140
120
100
80
0
100
200
300
400
500
600
Projectile energy (MeV/nucleon)

Fig. 3

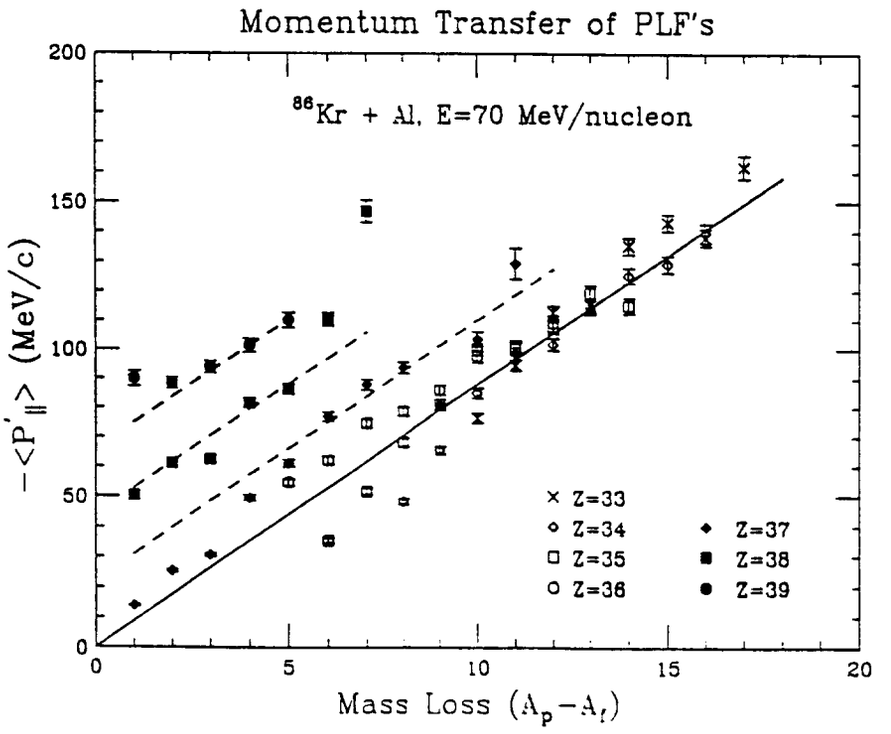
Momentum Transfer of PLF's
^{86}Kr + Al, E=70 MeV/nucleon
$-\langle P'_{\parallel} \rangle$ (MeV/c)
200
150
100
50
0
0
5
10
15
20
Mass Loss ($A_p - A_f$)
Z=33
Z=34
Z=35
Z=36
Z=37
Z=38
Z=39

Fig. 4

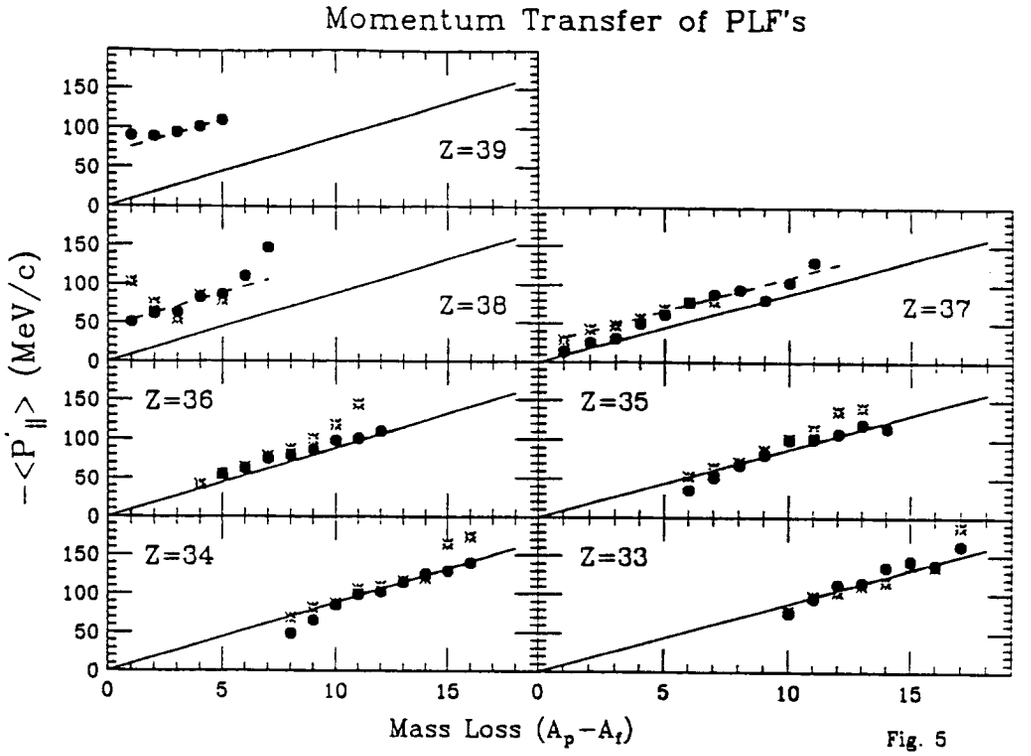
Momentum Transfer of PLF's
Z=39
Z=38
Z=37
Z=36
Z=35
Z=34
Z=33
$-\langle P'_{\parallel} \rangle$ (MeV/c)
Mass Loss ($A_p - A_f$)

Fig. 5

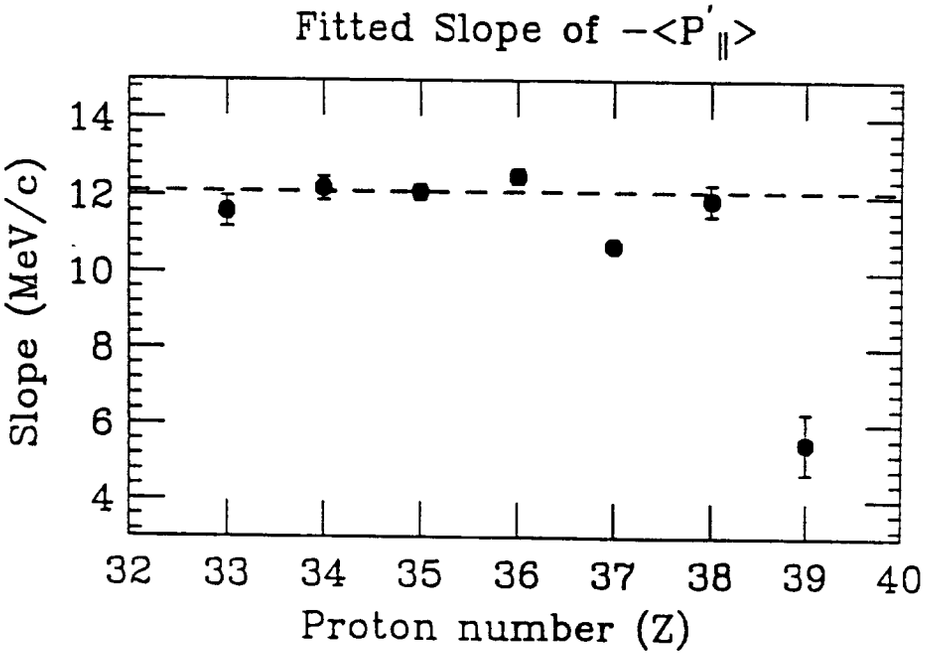
Fitted Slope of $-\langle P'_{\parallel} \rangle$
Slope (MeV/c)
Proton number (Z)

Fig. 6

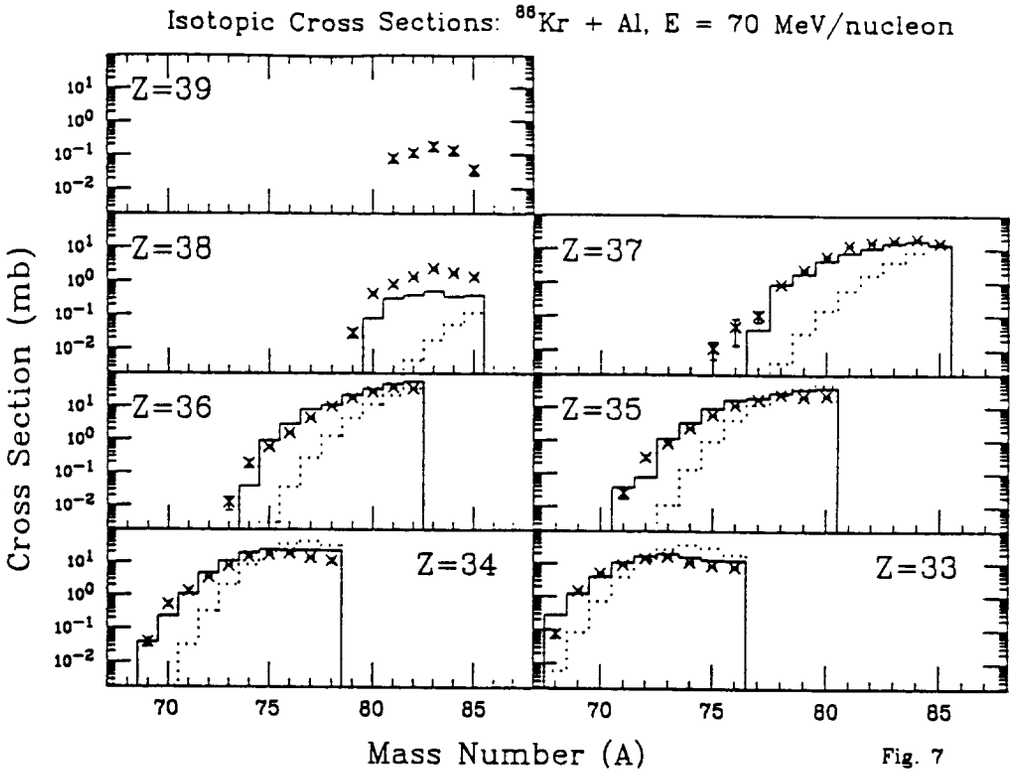
Isotopic Cross Sections: ^{86}Kr + Al, E = 70 MeV/nucleon
Z=39
Z=38
Z=37
Z=36
Z=35
Z=34
Z=33
Cross Section (mb)
Mass Number (A)
70
75
80
85

Fig. 7